J. Fluid Mech. (2010), *vol.* 656, *pp.* 507–529.
doi:10.1017/S0022112010001357

Acoustic and flow fields of an excited high Reynolds number axisymmetric supersonic jet

M. SAMIMY†, J.-H. KIM, M. KEARNEY-FISCHER AND A. SINHA

Gas Dynamics and Turbulence Laboratory, Department of Mechanical Engineering, The Ohio State University, 2300 West Case Road, Columbus, OH 43235-7531, USA

(Received 30 July 2009; revised 4 March 2010; accepted 11 March 2010; first published online 14 June 2010)

An axisymmetric perfectly expanded Mach 1.3 jet, with a Reynolds number based on the nozzle exit diameter (Re_D) of 1.1×10^6 and turbulent boundary layer at the nozzle exit, was excited using localized arc filament plasma actuators over a wide range of forcing Strouhal numbers (St_{DF}). Eight actuators distributed azimuthally were used to excite azimuthal modes $m = 0$–3. Far-field acoustic, flow velocity and irrotational near-field pressure were probed with a three-fold objective: (i) to investigate the broadband far-field noise amplification reported in the literature at lower speeds and Re_D using excitation of $m = 0$ at low St_{DF}; (ii) to explore broadband far-field noise suppression using excitation of $m = 3$ at higher St_{DF}; and (iii) to shed some light on the connection between the flow field and the far-field noise. The broadband far-field noise amplification observed is not as extensive in amplitude or frequency range, but still sufficiently large to be of concern in practical applications. Broadband far-field noise suppression of 4–5 dB at 30° polar angle peak frequency, resulting in approximately 2 dB attenuation in the overall sound pressure level, is achieved with excitation of $m = 3$ at $St_{DF} \sim 0.9$. Some of the noteworthy observations and inferences are (*a*) there is a strong correlation between the far-field broadband noise amplification and the turbulence amplification; (*b*) far-field noise suppression is achieved when the jet is forced with the maximum jet initial growth rate frequency thus limiting significant dynamics of structures to a shorter region close to the nozzle exit; (*c*) structure breakdown and dynamic interaction seem to be the dominant source of noise; and (*d*) coherent structures dominate the forced jet over a wide range of St_{DF} (up to ~ 1.31) with the largest and most organized structures observed around the jet preferred mode St_{DF}.

1. Introduction

Jet noise has been an environmental nuisance since the advent of jet engines. The problem has become more acute due to the ever increasing number of flights, the encroachment of residential establishments around airports and increasingly stricter environmental regulations. Consequently, jet noise could gradually become a key factor in the commercial viability of jet engines. In addition, concerns for

† Email address for correspondence: samimy.1@osu.edu

environmental noise are even starting to impact military aircraft, as the newer high-performance military aircraft are significantly noisier than their predecessors.

Aircraft noise is composed of many components (e.g. noise from fan, combustor, turbine, jet, etc.). Each component possesses certain characteristics that are used for its identification in the acoustic signature of the aircraft. The components have been separately studied in laboratories and corresponding models have been developed and tested over several decades. However, the laboratory and computational models of jet noise often significantly underpredict the broadband jet noise from an actual jet engine (Deneuville & Jacques 1977; Moore 1977*a*; Lu 1983; Tanna & Ahuja 1985). This perplexing issue has challenged researchers for several decades.

Linear instability analysis from the 1960s and 1970s had clearly shown that the jet acts like a band-limited amplifier (e.g. Michalke 1965). Therefore, it was suspected that other noise components, especially those with pure tone components such as the fan, turbine or combustor, were interacting with and exciting the jet thereby elevating the broadband noise in the actual jet engines (Moore 1977*b*; Crighton 1981). However, if such an interaction is at work, it is quite complex, not well understood, and is not taken into account in the predictive models for jet noise. Instability analysis results along with the observation of large-scale coherent structures in free shear layers and jets in the 1970s (Crow & Champagne 1971; Brown & Roshko 1974) fuelled two lines of thought: (i) excitation of these structures by internal engine noise sources could be responsible for the elevated noise in jet engines, and (ii) these structures could be actively controlled by external sources to improve the understanding of the broadband noise amplification in jet engines, and potentially even for jet noise mitigation (Crow & Champagne 1971; Bechert & Pfizenmaier 1975; Moore 1977*a*; Kibens 1980; Crighton 1981). In addition, researchers began to use low-amplitude tonal forcing to organize the structures and to provide a reference phase/time in experimental measurements to study the physics of these structures in free shear layers and jets (Ho & Huerre 1984). These findings and thoughts created tremendous research activities in the 1970s and 1980s in active control of jets (e.g. Crow & Champagne 1971; Bechert & Pfizenmaier 1975; Moore 1977*a*; Morrison & McLaughlin 1979; Kibens 1980; Zaman & Hussain 1980, 1981; Crighton 1981; Hussain 1983, 1986; Ho & Huerre 1984; Ahuja & Blakney 1985; Bridges & Hussain 1987, 1992; Hussain & Hasan 1985).

An axisymmetric jet has two length scales: the nozzle exit diameter and the nozzle exit boundary layer momentum thickness. Detailed instability analysis (Michalke 1965; Michalke & Fuchs 1975) and experimental results (Zaman & Hussain 1981) show that the shear layer is receptive to perturbations over a large range of frequencies. Maximum growth rate is achieved when the shear layer is forced at $St_{\theta F}$ $(= f_F\theta/U_j$, where f_F is the forcing frequency, θ is the nozzle exit boundary layer momentum thickness and U_j is the nozzle exit velocity) of around 0.017 (Michalke 1965; Zaman & Hussain 1981) and the roll up of the structures and maximum growth occur in a naturally growing shear layer at $St_\theta \sim 0.012$ (Zaman & Hussain 1981). The jet column (or the jet preferred) mode is also unstable to perturbation over a range of Strouhal numbers. In a low Re_D jet with a laminar initial shear layer, the initial instability waves roll up into large-scale structures that go through successive pairings. The passage frequency of these structures is halved after each pairing event and as a result the initial shear layer instability and the jet column instability are coupled (Kibens 1980). No such coupling has been observed in jets with turbulent initial shear layer.

In addition to the initial shear layer and the jet preferred mode instabilities, axisymmetric jets are susceptive to azimuthal mode instability. The primary parameter affecting the development of azimuthal modes is D/θ (Cohen & Wygnanski 1987;

Corke, Shakib & Nagib 1991). In the current work, with $D/\theta \sim 250$, the jet is receptive to many forcing azimuthal modes, consistent with the results in the literature.

The results in the literature appear to be consistent and show broadband turbulence amplification as well as far-field noise amplification in jets excited with a pure tone at a Strouhal number around the jet preferred mode ($St_{DF} = f_F D/U_j \sim 0.3$, where D is the nozzle exit diameter). The broadband amplification in turbulence and far-field noise was obtained regardless of whether the nozzle exit boundary layer was laminar or turbulent (Bechert & Pfizenmaier 1975; Moore 1977*a*; Crighton 1981; Hussain & Zaman 1981; Ahuja & Blakney 1985).

In using much higher St_{DF} excitation (>1.5), the results heavily depend on the state of the boundary layer. In low Re_D jets with laminar nozzle exit boundary layer, broadband turbulence suppression (Zaman & Hussain 1981) as well as far-field noise suppression (Kibens 1980; Hussain & Hasan 1985) has been observed with forcing Strouhal number within the jet initial shear layer instability range ($St_{\theta F} \sim 0.012$ to 0.017. When the boundary layer at the nozzle exit is turbulent, Zaman & Hussain (1981) observed no broadband turbulence suppression, and Moore (1977*a*) observed a suppression of about 1 dB in the far-field noise. The broadband suppression seemed to be almost uniform over the entire spectral frequency range and also over a large range of polar angles with respect to the jet axis.

All the works cited above used acoustic drivers for the excitation. While these drivers have been used successfully for flow control in low-speed and low Re_D jets, they normally lack the amplitude and bandwidth required in high-speed and high Re_D jets (Crow & Champagne 1971; Kibens 1980). There are some recent works in active jet noise control that use microjets, and thus streamwise vorticity rather than instability mechanism manipulation (e.g. Arakeri *et al.* 2003; Castelain *et al.* 2007; Alkislar 2009). Over the past several years, we have developed a class of high-amplitude and high-bandwidth plasma actuators called localized arc filament plasma actuators (LAFPAs) (Samimy *et al.* 2004, 2007*b*; Utkin *et al.* 2007). The objective of this work is to utilize these plasma actuators in a perfectly expanded supersonic jet to revisit some of the issues discussed above. In addition, these actuators are capable of forcing the jet with the higher St_{DF} and azimuthal modes that appear to be crucial actuator characteristics for realization of noise mitigation.

There is a significant body of literature accumulated over three decades on the receptivity of free shear layers and jets to external perturbations (e.g. Tam 1978; Ahuja 1985; Crighton 1985; Bechert 1988; Bechert & Stahl 1988; Barone & Lele 2005). There is agreement among researchers on some aspects and disagreement on other aspects of receptivity. The following ideas have general agreement: (i) the receptivity is maximum where the shear layer is initiated, namely at the nozzle or splitter plate edge; (ii) the receptivity is in general higher when the perturbations are located upstream rather than downstream of the nozzle/splitter plate edge; and (iii) jets and free shear layers with laminar initial shear layers are more receptive than those with turbulent initial shear layers.

The disagreement on the receptivity is on whether a scattering edge, such as the nozzle/splitter plate is required for receptivity. For example, Tam (1978) and Ahuja (1985) support continuous coupling (which means that perturbations could be introduced at any downstream location in the shear layer), while Crighton (1985) and Bechert (1988) support the trailing-edge interaction theory based on the Kutta condition. Designing an experiment to completely isolate one effect from the other has proven to be unattainable, and thus the different opinions continue. A brief review of most of the past work can be found in Barone & Lele (2005), where they use a

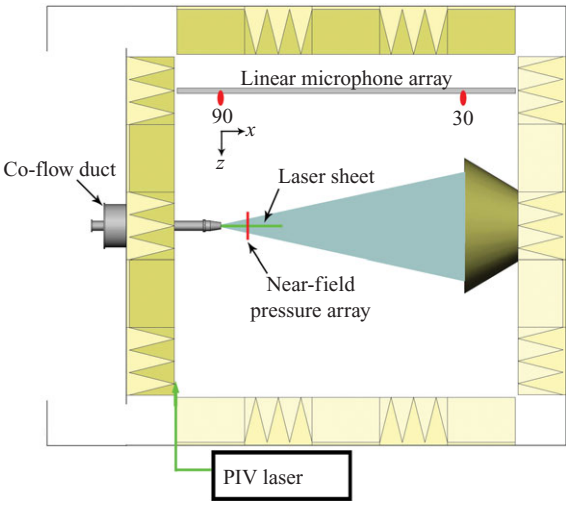

FIGURE 1. (Colour online) Schematic of jet and anechoic chamber.

combined numerical and theoretical technique to show that there could be receptivity nodes near the splitter plate/nozzle edge due to superposition of the incident and scattered fields.

The actuators in the current experiment are located as close as physically possible to the beginning of the jet shear layer to maximize the receptivity.

2. Experimental facility and techniques

2.1. *Flow facility*

All the experiments were carried out at the Gas Dynamics and Turbulence Laboratory (GDTL) at the Ohio State University. The jet at GDTL is created using compressed air and a contoured Mach 1.3 nozzle of exit diameter $D = 25.4$ mm, which is designed using the method of characteristics. The nozzle is operated in the perfectly expanded regime with Re_D of about 1.1×10^6. The compressed air is supplied to the stagnation chamber of the jet facility, discharged horizontally through the nozzle into an anechoic chamber and then passes through an exhaust system to the outdoors (figure 1).

2.2. *Flow and acoustic diagnostic techniques*

Far-field sound pressure level is measured using 1/4 in. B&K 4939 microphones located from 25° to 90° polar angles with respect to the jet axis, but for brevity only representative results at 30° and 90° will be presented in this paper. The far-field acoustic results are scaled to a distance of 80 jet diameters. The acoustic signal from each microphone is band-pass filtered from 20 Hz to 100 kHz, amplified by B&K Nexus 2690 conditioning amplifiers and acquired using National Instruments A/D boards and LabView software. The frequency response of the microphones is flat up to 80 kHz with the microphone grid cover removed. Blocks of data are collected at 200 kHz with 8192 data points per block producing a spectral resolution of 24.4 Hz. An average sound pressure level spectrum is obtained using 100 blocks of data.

For irrotational near-field pressure measurements, a circular array of 8 Kulite pressure transducers (model XCQ-062-25A) is used. Pressure signals are amplified, low-pass filtered at 100 kHz and acquired using an eight channel National Instrument A/D card. The sampling parameters are the same as for the acoustic data.

A LaVision particle image velocimetry (PIV) system with a 2048×2048 pixel resolution camera is used for two-component (streamwise and radial) velocity measurements on an axial plane passing through the jet centreline. A Spectra Physics Model SP-400 dual head Nd:YAG laser is used as the light source for both PIV and flow visualization. For most of the streamwise velocity field measurements, the spatial resolution is about 2.2 mm. The laser sheet thickness is less than 0.3 mm. The time separation between two consecutive PIV images is 1.8 μs. The jet plume is seeded with liquid droplets atomized by a four-jet LaVision atomizer. A 381 mm diameter duct is placed around the jet to generate a very low speed ($\sim 0.8\,\%$ of the jet exit velocity) co-flow (see figure 1). The co-flow is seeded by a fogger to avoid statistical bias in the measurements, as well as spurious velocity vectors in the entrained air that has not mixed with the jet yet. The average droplet size is 0.7 and 0.25 μm for the jet flow and co-flow, respectively. Turbulence statistics are obtained using 700 image pairs – convergence of second-order turbulence statistics is achieved with 600–650 image pairs.

The flow is visualized using scattering of light from a laser sheet passing through the centreline of the jet. The light scattering moisture particles are formed in the mixing layer of the jet when the moist and warm ambient air is entrained into the jet and mixed with the cold but dry jet air. The scattered laser light is captured by a Princeton Instrument Pixis CCD camera. Instantaneous planar images of the jet with 9 ns exposure time are acquired. In this visualization technique, a major portion of the mixing layer is visualized since no condensation occurs in the jet core or the ambient air.

2.3. *Plasma actuators and the forcing mechanism*

The concept and earlier development of LAFPAs are presented in Samimy *et al.* (2004). The latest development and characterizations of LAFPAs, as well as the differences between LAFPAs and other plasma-based actuators, are given in Utkin *et al.* (2007) and Samimy *et al.* (2007*b*). A pair of electrodes, one attached to ground and the other to a voltage source with several kV capabilities, constitutes an LAFPA. A boron nitride nozzle extension with an inner diameter of 25.4 mm and thickness of ~ 19 mm is used to hold the actuators. Eight actuators are distributed uniformly around the nozzle extension perimeter approximately 1 mm upstream of the exit. The centre-to-centre distance between the two electrodes in an LAFPA is 4 mm. When the voltage across a pair of electrodes is ramped up and reaches the breakdown voltage, the air between the electrodes breaks down and an electric arc is established. Right after the breakdown, the voltage across the electrodes drops to a few hundred volts and remains at that level until the voltage source is disconnected. The frequency and duty cycle are controlled independently for each actuator and can be changed from near zero to 200 kHz, and from 3 % to 50 %, respectively. With the eight actuators, simple azimuthal modes from 0 to 3 and mixed modes 1, 2 and 4 can be excited.

Our most recent results show that the complete breakdown of the air is crucial for the control. Beyond the breakdown, the duty cycle has also some influence on the effectiveness of control. For the present work, the following empirical relation has been obtained experimentally and used:

$$\text{duty cycle}\,(\%) = \begin{cases} 0.6(f_F/1000) + 2 & \text{if } f_F \leqslant 30\,\text{kHz}, \\ 0.29(f_F/1000) + 11.42 & \text{if } f_F > 30\,\text{kHz}, \end{cases} \tag{1}$$

where f_F is the forcing frequency in Hz.

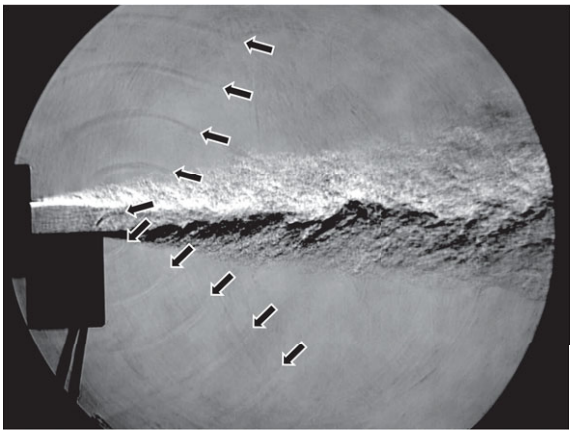

FIGURE 2. An instantaneous schlieren image of a rectangular Mach 0.9 jet showing the compression waves (indicated by arrows) generated by LAFPAs.

A circular groove of 1 mm width and 0.5 mm depth is used to shelter the plasma. The tips of the electrodes are housed within this groove, which is located approximately 1 mm upstream of the nozzle extension exit. The short duration and harsh high-temperature environment of the plasma pose challenges for any accurate measurements of perturbations imparted to the flow by the actuators. We have used nitrogen emission spectroscopy to measure the average temperature of the plasma, which depends on the frequency and duty cycle of the operation. The temperature, averaged over the spatial extent of the plasma (approximately 1 mm wide and 4 mm long) and over several pulses, varies from a few hundred to about 1200°C (Kim *et al.* 2009*b*) depending upon the duty cycle.

Figure 2 shows an instantaneous schlieren image (with approximately 1 μs exposure time) of a Mach 0.9 jet exhausting from a rectangular nozzle with exit height and width of 12.7 mm and 38.1 mm, respectively. The nozzle bottom plate was extended for about 25.4 mm downstream of the nozzle exit and four actuators were distributed uniformly in the spanwise direction in a groove of 1 mm width and 0.5 mm depth. To improve the schlieren image quality of the compression waves generated by the actuators, all four actuators were operated in phase at a frequency of 20 kHz and a duty cycle of 14 %. The average temperature of the plasma was approximately 600°C. One compression wave within the jet and four on the upper side of the jet, after passing through the jet, are clearly visible in the image. These waves have distorted wavefronts due to the effects of the convecting shear flow. There are also five visible waves on the lower and outside of the jet, with unaffected wavefronts. The wavelength of the forcing signal is 18 mm, which agrees with the wavelength seen in the image.

The jet is known to be receptive to thermal, aerodynamic and acoustic perturbations (Moore 1977*a*). With LAFPAs, the initial perturbation is thermal. However, the flow is compressible and the rapid microsecond time-scale localized heating generates a compression wave, as shown in figure 2. Our earlier unsteady quasi-one-dimensional model of the arc filament showed that the rapid localized heating generated compression waves that were steepened in a short period ($\sim$10 μs) and in a short distance ($\sim$3 mm) to become a stronger compression wave (Utkin *et al.* 2007). It is unclear at this time whether it is the thermal perturbation, the pressure perturbation or a combination of the two that is coupled to the flow.

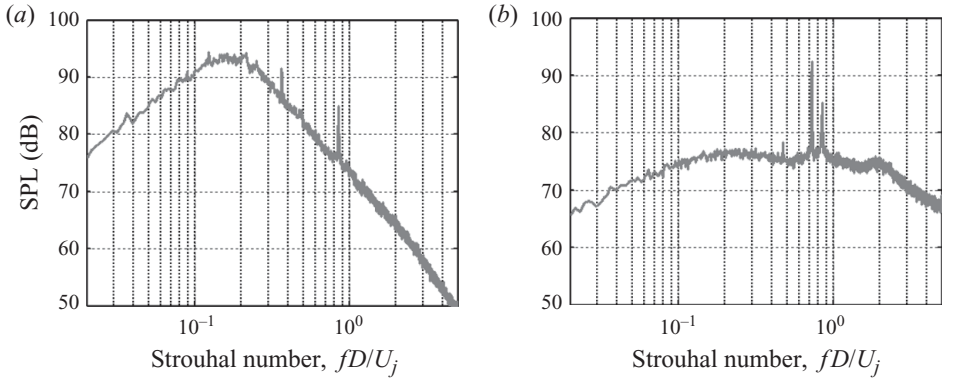

FIGURE 3. Far-field SPL for the baseline Mach 1.3 perfectly expanded axisymmetric jet at (*a*) 30°, (*b*) 90° with respect to the jet axis.

3. Experimental results and discussion

3.1. *Boundary layer characteristics at nozzle exit*

The nozzle is 152 mm long with a contraction ratio of 3 providing a gentle expansion of the flow within the nozzle. The 19 mm long nozzle extension provides relaxation to the boundary layer developed within the nozzle. With this arrangement and with high Re_D, the boundary layer is expected to be turbulent. The boundary layer thickness is estimated to be about 1 mm, which makes it almost impossible to make detailed measurements within the boundary layer to determine its characteristics. Our most recent hot-wire measurements show that the boundary layer is turbulent in a subsonic jet from a converging nozzle attached to the same facility over a Mach number range of 0.25–0.65 and Re_D range of 200 000–600 000 (Kearney-Fischer, Kim & Samimy 2009*b*). The best guess at this time is that the boundary layer and momentum thicknesses in the current work are of the order of 1 mm and 0.1 mm, respectively.

3.2. *Excitation of* $m = 0$ *mode*

Experimental results for far-field acoustic, flow velocity and irrotational near-field pressure will be presented and discussed for the $m = 0$ excitation. With a couple of exceptions, this is the excitation mode that has always been used in the literature for jet excitation.

3.2.1. *Far-field acoustic results*

Figure 3 shows the far-field sound pressure level (SPL) spectra at 30° and 90° with respect to the jet axis for the baseline jet. The Strouhal number ($St_D = fD/U_j$) for the broadband peak attributed to the dynamics of large-scale structures is around 0.2. This broadband peak normally varies between St_D of 0.15 and 0.3 and becomes sharper at very low Re_D (Morrison & McLaughlin 1979). The nozzle is designed using the method of characteristics for wave-free flow in the perfectly expanded operating regime. However, it is an inviscid calculation and cannot account for the boundary layer growth within the nozzle. Therefore, even in the perfectly expanded operating regime, there are weak waves in the jet. These waves interact with the large-scale turbulence structures and generate acoustic waves, which travel upstream and interact with the thick nozzle attachment used to house the plasma actuators. This process establishes a feedback loop, which is responsible for the screech tones shown in the figure. The tone at $St_D \sim 0.85$ appears at both 30° and 90°, but the

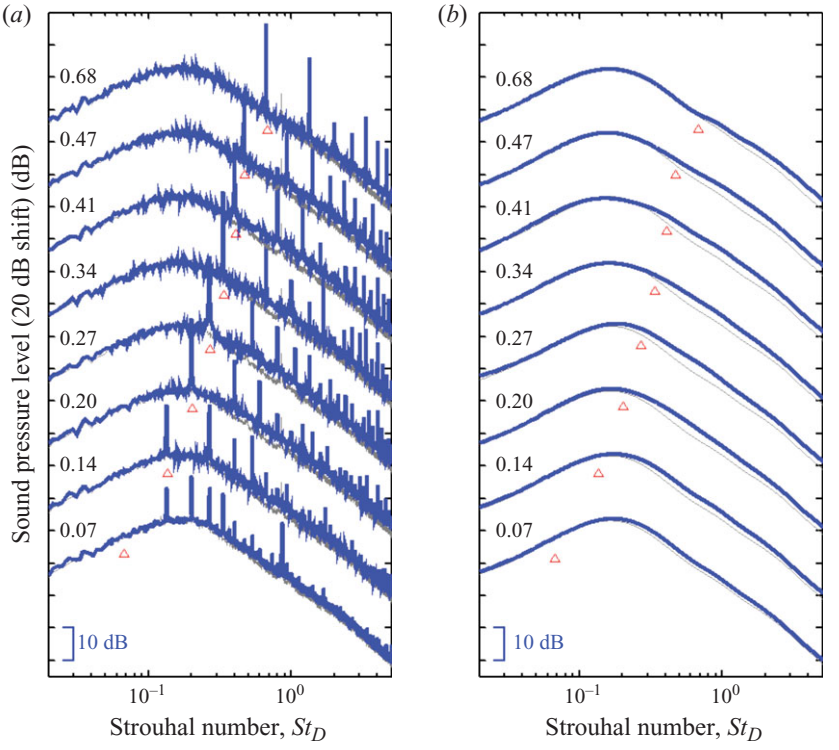

FIGURE 4. (Colour online) Far-field SPL at 30° for baseline jet (thin grey line) and for jet with $m = 0$ excitation and low St_{DF}: (*a*) with excitation tones retained; (*b*) with excitation tones removed. Each spectrum is displaced vertically by 20 dB for legibility and St_{DF} is shown above each individual spectrum.

strongest tone at $St_D \sim 0.73$ appears only at 90°. It is known that the screech tone is radiated mostly in the upstream direction. There are also two weaker peaks at $St_D \sim 0.37$ and ~ 0.47 at 30° and 90°, respectively. Azimuthal decomposition of the near-field pressure, to be discussed later, reveals that these two peaks correspond to $m = 1$ and 0 modes, respectively. One or more of several screech modes could appear in a given jet, depending upon the jet operating conditions (Norum 1983; Raman 1999). In addition to the screech modes, their multiple harmonics are also seen in jets (Norum 1983). The screech tones in the current work are weak, but they could be quite strong in imperfectly expanded jets, which could set up a competition for energy and growth between the excitation tone and the screech modes, thereby reducing the control authority (Kim & Samimy 2009).

Figure 4 shows the far-field SPL at 30° with $m = 0$ mode excitation for various St_{DF} covering the typical jet preferred mode St_D range (~ 0.2–0.6). The figure shows the spectra with and without the excitation-related tones. The tone removal was carried out in two steps. First, the tone level was significantly reduced by using two to three passes of a five-point moving-average algorithm. Then a very high-order (30th to 35th) polynomial was fitted to the spectrum to remove the tones, which also served to smooth the spectrum. On each spectrum, a triangular symbol shows the St_{DF}. Except for the excitation at the lowest St_{DF} (0.07), the forcing tone appears in every spectrum. All other tones appearing in the spectrum are various harmonics of the forcing tone, similar to the results in the literature (Bechert & Pfizenmaier 1975). The

absence of the forcing tone at St_{DF} of 0.07 appears to be a result of the mismatch of the excitation wavelength and the jet length scales, as the forcing wavelength at this frequency is approximately 9 jet diameters, which is longer than the jet column itself.

Jet excitation research was motivated in the 1970s and 1980s by the higher jet broadband noise observed in an actual jet engine in comparison with that of laboratory jets (Moore 1977*a*; Crighton 1981). Therefore, the forcing tone and its harmonics were often removed (Moore 1977*a*) for the ease of observation of the changes in the broadband noise. Similar to the results in the literature obtained using acoustic drivers, forcing the jet with St_{DF} over the range of jet preferred mode causes far-field broadband noise amplification, with the maximum amplification around $St_{DF} \sim 0.27$. There are two major differences between the results in figure 4 and those in the literature (Moore 1977*a*; Jubelin 1980; Crighton 1981): (i) the amplification is not over the entire frequency range, but limited to higher frequencies (higher than the peak frequency and moving up as St_{DF} increases); (ii) the maximum amplification (approximately 4–5 dB at St_{DF} of 0.27) is not as high as the 10 dB reported in the literature. Moore's results showed that the level of amplification almost linearly depended on the excitation level above a certain threshold. The variations in the broadband amplification level in different laboratories are much higher than those in actual engines. This has been attributed to the use of acoustic drivers in laboratories, which lack the ability to produce excitation signals large enough to produce saturation while internal processes in an actual engine can produce very high levels of excitation. We do not have a straightforward control on the excitation level as was discussed in § 2.3.

Figure 5(*a*) shows the far-field SPL at 30° with $m = 0$ mode at higher St_{DF}. For this range of frequencies, the forcing frequency and its harmonics appear in every spectrum (not shown). The trend of reduced broadband amplification level and the shift in the onset of the amplification to higher St_D with increasing St_{DF} continues. However, a second trend of broadband noise suppression around the far-field noise peak appears at St_{DF} of 0.81. The suppression level as well as the range of frequencies over which the suppression is observed is maximized at St_{DF} of about 1.8, followed by a reverse trend at high St_{DF}. The maximum suppression is about 2–3 dB. These results are similar to our recent results in a high Re_D Mach 0.9 jet (Samimy *et al.* 2007*a*). These trends are also similar to those in the literature to some degree. For example, Moore (1977*a*) reported a noise suppression of about 1 dB with St_{DF} of higher than 1.6 in an unheated Mach 0.4 jet.

Figure 5(*b*) shows the far-field acoustic results at a 90° polar angle for several St_{DF}. Both screech tones are suppressed by forcing (not shown), which is typical when an external asymmetry (e.g. a tab/chevron) or an azimuthal non-uniformity (as in the present case) is introduced. Similar to the 30° polar angle results, the forcing frequency and its harmonics appear in every spectrum (not shown). Noise suppression of up to 3–4 dB is observed in the mid range frequencies for St_{DF} between 1.5 and 2.4. Above or below this range, the suppression level is minimal. These results are similar to those of Jubelin (1980) who showed a suppression of up to 2 dB in a heated jet of 600 K and Mach number of 0.47 with St_{DF} of 2.4–2.9. It should be noted that our recent results in a heated Mach 0.9 jet show significantly higher noise suppression in the heated jet (Kearney-Fischer, Kim & Samimy 2009*a*).

There is no definite answer to the question of what is generating noise in a jet when the large-scale structures are moving at a subsonic speed (see recent review papers Tam 1998; Jordan & Gervais 2008). Lighthill (1952) in his seminal formulation of jet noise theory assumed that Reynolds stresses are the major source of jet noise. Others have

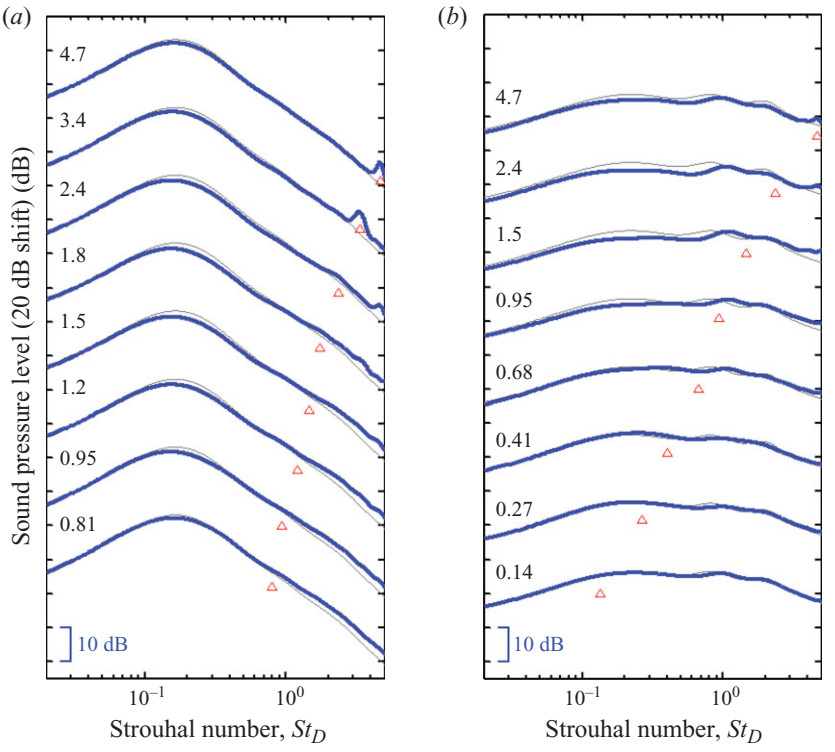

FIGURE 5. (Colour online) Far-field SPL for the baseline jet (thin grey line) and for jet with $m = 0$ excitation: (*a*) at 30° and higher St_{DF}; (*b*) at 90° over a large range of St_{DF}.

used a growing and decaying wave packet as a noise source (e.g. Ffowcs-Williams & Kempton 1978; Reba *et al.* 2005; Gudmundsson & Colonius 2009). The rapid growing and decaying of instability waves were determined to be the major noise source in very low Re_D supersonic jets with no Mach wave radiation (Morrison & McLaughlin 1979). Hileman *et al.* (2005) used simultaneous real-time flow visualization and acoustic measurements to show that strong interactions followed by disintegration of large-scale flow structures in the present jet are responsible for the peak noise radiation. In low Re_D jets with laminar boundary layer at the nozzle exit, vortex pairing has been shown to be the major source of jet noise (e.g. Kibens 1980). Bridges & Hussain (1987, 1992) used a low-speed jet with different initial conditions to look into the role of vortex pairing on the far-field noise and concluded that vortex pairing cannot be the dominant noise source in practical jets. Hussain (1983, 1986) has argued that structure breakdown via reconnection (rather than pairing) is the dominant noise source mechanism. He has offered the rapid breakdown of ring vortices into azimuthally distributed substructures and their interaction as the main source of jet noise. Qualitatively, one can argue that all these mechanisms, one way or another, are related to the dynamics of large-scale structures in the jet. Forcing the jet at St_{DF} close to the jet preferred mode has been shown to generate strong and coherent large-scale structures even in very high Re_D Mach 1.3 and 0.9 jets (Samimy *et al.* 2007*b*; Kim *et al.* 2009*a*); this is further demonstrated below. Therefore, it is reasonable to assume that such forcing would increase the dynamics of large-scale structures and thus would increase the broadband noise. The consistent results in the literature seem

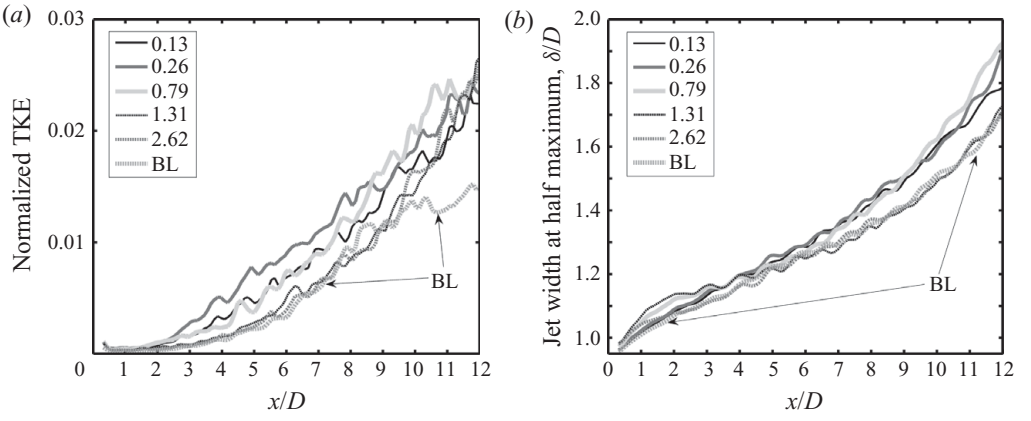

FIGURE 6. (*a*) Normalized centreline TKE, and (*b*) jet width for baseline jet (BL) and excited jet with $m = 0$ for various St_{DF}.

to confirm this notion. The case of noise suppression using higher St_{DF} is not as clear, and will be further discussed later.

3.2.2. *Flow results*

Figure 6(*a*) shows jet centreline two-component turbulent kinetic energy (TKE) normalized by U_j^2 (normalized TKE) for the baseline jet and several forced jets. The centreline turbulence is significantly amplified over the entire axial measurement domain for the lower three St_{DF}, with the maximum amplification at the St_{DF} near the jet preferred mode. These results are consistent with those in the literature (Moore 1977*a*; Hussain & Zaman 1981) and link turbulence amplification with far-field noise amplification. The two highest St_{DF} do not show any effect until $x/D \sim 9.5$, beyond which turbulence is increased, which is consistent with the results of Zaman & Hussain (1981) in low Re_D jets with a turbulent boundary layer at the nozzle exit. The result at St_{DF} of 0.79 resembles that of Zaman & Hussain (1980) in a jet with tripped boundary layer, in which St_{DF} was around 0.85. They showed higher jet centreline turbulence intensity with St_{DF} of 0.3 upstream and with St_{DF} of 0.85 further downstream.

Figure 6(*b*) shows the normalized jet width at half-maximum velocity (jet width, hereafter). Several distinct behaviours are observed. The jet initial growth rate for the two lowest St_{DF} is similar to that of the baseline case, but their growth rate further downstream is much higher than that of the baseline case. Recall from the results in figure 4 that these two forcing cases, especially the one with St_{DF} of 0.27, significantly increase the broadband noise at 30° polar angle. The initial growth rate for the other three St_{DF} increases with St_{DF}, reaches a maximum at St_{DF} of 1.31 and then decreases. However, the growth rate further downstream for the two highest St_{DF} is very similar to that of the baseline case. Recall from figures 4 and 5 that the broadband noise is significantly decreased with these St_{DF}, especially with St_{DF} of 1.31, at both 30° and 90° polar angles. The downstream growth rate for St_{DF} of 0.79 is similar to that of the two lower St_{DF}. Recall from figures 4 and 5 that for this forcing case, there is a small broadband noise amplification. As seen in figure 6(*a*), the downstream amplification of TKE for this case is even above that of $St_{DF} = 0.27$. These trends, except for that of $St_{DF} = 0.79$, are consistent with the interpretation of dynamic interaction of large-scale structures being responsible for the far-field noise. The case of $St_{DF} = 0.79$ will be further discussed later.

The results in the literature show consistently that forcing the jet with St_{DF} close to that of the jet preferred mode increases the broadband jet turbulence as well as the broadband far-field noise, regardless of the jet's Re_D or the status of the boundary layer at the nozzle exit. The current results with a supersonic jet, much higher Re_D, and turbulent boundary layer at the nozzle exit show general agreement with the results in the literature. However, interpreting the results in the literature on the effects of forcing at higher St_{DF} is not as straightforward. For low Re_D jets with a laminar nozzle exit boundary layer, forcing the jet with an St_{DF} associated with the initial shear layer instability ($St_{\theta F} \sim 0.01$–0.02) results in suppression of turbulence (Zaman & Hussain 1981), the irrotational near-field pressure (Kibens 1980) and the far-field sound pressure level (Kibens 1980; Hussain & Hasan 1985). With laminar initial shear layer, the initial instability wave rolls up into vortices, which go through successive pairings (Ho & Huerre 1984). Zaman & Hussain (1981) provide results in support of the idea that forcing, especially with the maximal initial growth rate Strouhal number ($St_{\theta F} \sim 0.017$), promotes fast initial growth and early saturation. This results in suppression of the structures and turbulence when the boundary layer is laminar, but not when it is turbulent. Hussain & Hasan (1985) argued that this suppression of structures and turbulence is also the cause of the broadband suppression of noise. The current results with very high Re_D and turbulent initial boundary layer seem to follow the trends shown in the low Re_D jets. For example, the jet initial growth rate is maximal when higher St_{DF} is used (see figure 6*b*), and significant noise suppression is achieved, as shown in figures 4 and 5, similar to the results obtained by Hussain & Hasan (1985). This high Strouhal number forcing (resulting in noise suppression) is not associated with turbulence suppression, as shown in figure 6(*a*), which is again consistent with the results obtained by Zaman & Hussain (1981) in a low Re_D jet with tripped nozzle exit boundary layer.

High St_{DF} excitation of high Re_D jets produces noise suppression, but the suppression level is not as high as the amplification level seen in lower frequency forcing (Moore 1977*a*; Jubelin 1980). However, there are significant variations in the optimal St_{DF}. For example, Moore (1977*a*) showed a noise suppression of about 1 dB with St_{DF} of higher than 1.6. The current results show noise suppression with St_{DF} between 0.95 and 4.7, with the maximum suppression around St_{DF} of 2.0. Hussain & Hasan (1985), observing significant variation in the St_{DF} for noise mitigation, questioned the use of Strouhal number based on nozzle exit diameter rather than based on the nozzle exit boundary layer momentum thickness for high forcing frequencies. Unfortunately, the literature on high frequency forcing of high Re_D jets lacks sufficient information on the boundary layer characteristics to determine θ and to examine the correct scaling of the forcing Strouhal number. Assuming $St_{\theta F}$ to be between 0.01 and 0.02 for the optimum forcing Strouhal number for noise mitigation (Hussain & Hasan 1985), our result of optimal $St_{DF} \sim 2.0$ gives a boundary layer momentum thickness $\theta \sim 0.13$–0.26 mm. The lower values in this range seem to be approximately correct for our estimated boundary layer momentum thickness, as was discussed earlier.

Figure 7 shows ensemble-averaged flow images for the baseline jet and phase-averaged images for the jet excited with $m = 0$ for several St_{DF}. Several observations can be made: (i) The structures are not well organized in the St_{DF} of 0.13 case due to the mismatch of the forcing wavelength and the local jet scales. The observed structures (at $x/D \sim 3$ and 5) are probably associated with the screech tone at St_D of 0.47 in figure 3 (which is observed at the 90° polar angle in the far-field, and in the irrotational near-field pressure to be discussed next). (ii) The structures are well organized at St_{DF} of 0.26, which is close to the jet preferred mode from the acoustic

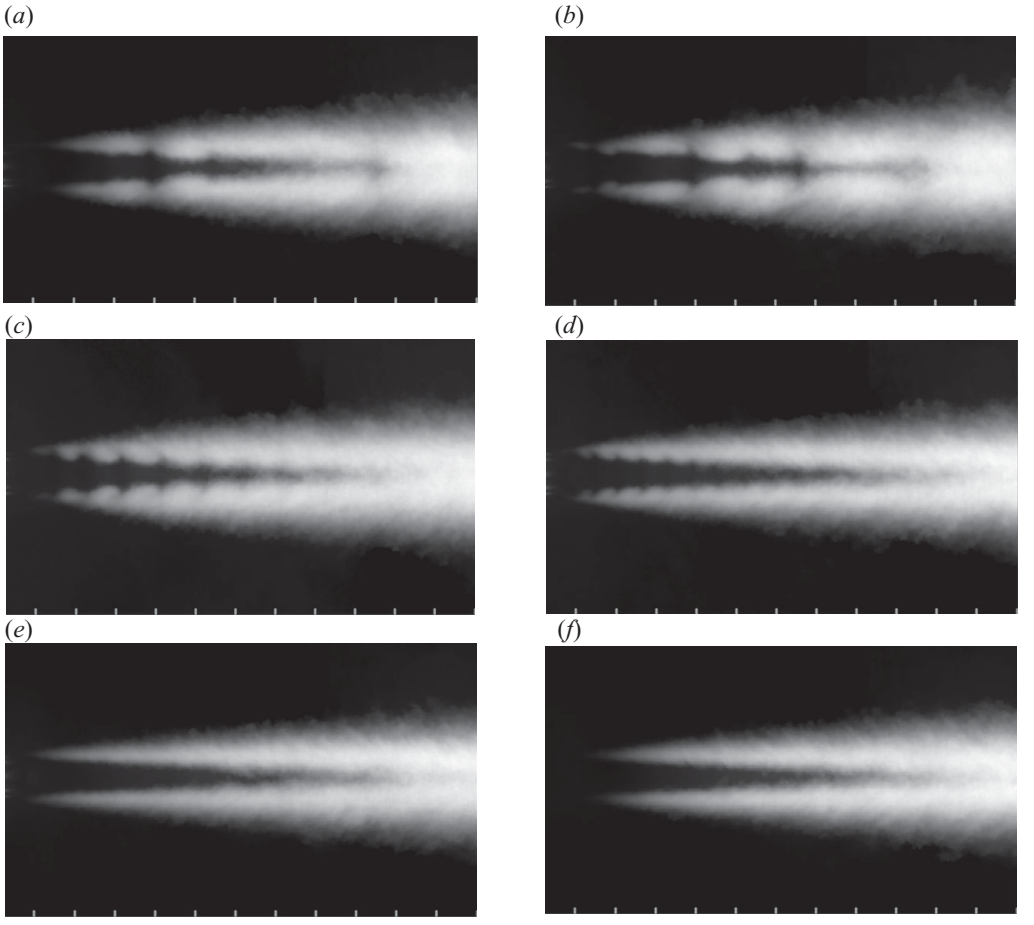

FIGURE 7. Phase-averaged flow images of the baseline jet (*f*) and excited jet with $m = 0$ for several St_{DF} (0.13 (*a*), 0.26 (*b*), 0.79 (*c*), 1.31 (*d*) and 2.62 (*e*)). Mixing intensity decreases from white to black.

results and produced maximum noise amplification as shown in figure 4. Surprisingly, these structures are quite elongated in the streamwise direction. (iii) Also remarkably, the structures are well organized even at as high an St_{DF} as 1.31. (iv) There are no observable structures, due either to their absence or their small size (beyond the resolution of the imaging system), at the highest St_{DF}.

Zaman & Hussain (1980) observed vortex pairing with a laminar or tripped turbulent boundary layer when a jet was excited with St_{DF} of around 0.85, whose subharmonic falls within the jet column mode. The location of pairing was around x/D of 2. The excitation at St_{DF} of 0.79 (figure 7*c*) falls into this category, but unfortunately, we cannot image the shear layer that close to the jet (due to the lack of particles for light scattering) to investigate any potential pairing. However, the irrotational near-field pressure to be discussed next shows subharmonic formation with St_{DF} close to 0.79; this is an indication of vortex pairing.

In a free shear layer with a laminar boundary layer at the nozzle exit, Ho & Huerre (1984) discussed a complex relation among the natural initial shear layer instability frequency, forcing frequency and the initial formation spacing of structures. In the

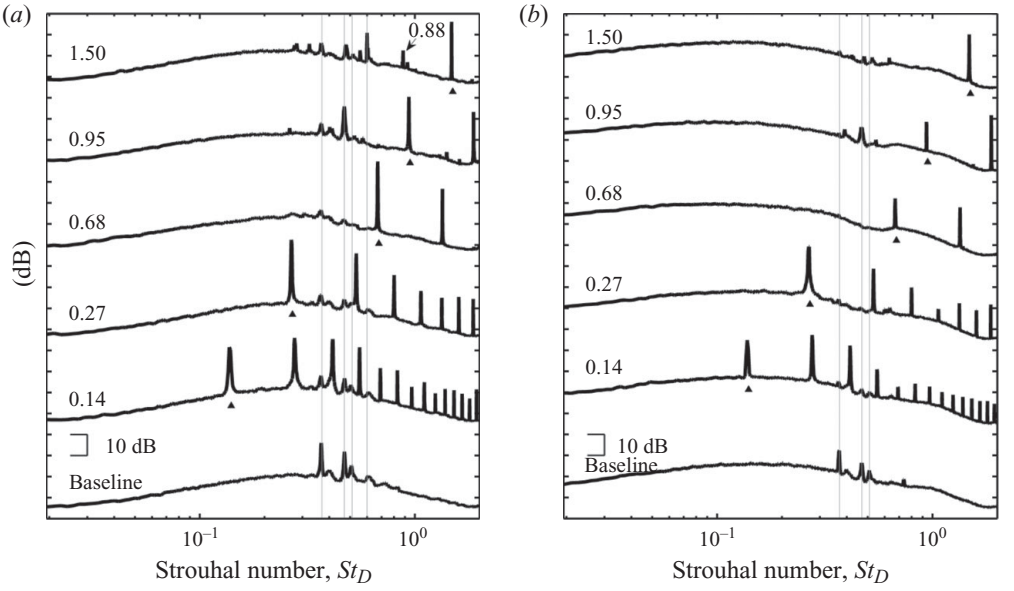

FIGURE 8. Near-field pressure spectra for the baseline jet and excited jet with $m = 0$ mode for several St_{DF} at $(x/D, r/D)$ of (*a*) (3, 1.25) and (*b*) (6, 1.49).

perfectly expanded Mach 1.3 jet of the current work with a high Re_D and turbulent boundary layer, Kim & Samimy (2009) used spatial correlation of PIV data to obtain structure spacing or wavelength (λ) and showed that all the data in the excited jet fit the following curve:

$$\frac{\lambda}{D} = \frac{a}{St_{DF}} + b, \tag{2}$$

where a and b are constants. From the structures observed in figure 7 and far-field noise results in figures 4 and 5, it seems that forcing the jet with higher frequencies organizes the structures into smaller structures (in comparison with larger but incoherent structures in the baseline jet) with weaker dynamic interactions and over shorter downstream distance, and results in noise suppression.

3.2.3. *Near-field pressure results*

Limited irrotational near-field pressure results were also obtained using a ring array with eight Kulite pressure transducers at two streamwise locations of $x/D = 3$ and 6. Several researchers have used such measurements in jets to provide insightful information (e.g. Hall *et al.* 2006; Suzuki & Colonius 2006; Tinney & Jordan 2008). Radially, the tips of the pressure transducers were located outside the shear layer in the irrotational field of the jet, at $r/D = 1.25$ and 1.49, respectively. The difference in radial location accounted for the $\sim 4.5^\circ$ half-angle flaring of the jet observed in the baseline jet.

Figure 8 shows pressure spectra (defined similarly to the sound pressure level with 20 μPa reference pressure and unit of dB) for the baseline jet and excited jet with $m = 0$ mode for several St_{DF}. The spectra are shown up to St_D of 2.0, as the resolution of pressure transducers may not be reliable at higher frequencies. In the baseline spectrum at $x/D = 3$, there are two relatively strong peaks at $St_D = 0.37$ and 0.47 that match the St_D of the screech tones shown in figure 3. These peaks along

with two weaker peaks at $St_D = 0.51$ and 0.60 are identified in figure 8 by thin lines for the ease of tracking these tones in the excited jet results. Three of these four peaks are also visible at the $x/D = 6$ location, but with lower amplitudes. While the microphones in the far field measure the radiated noise from the jet, the pressure transducers in the irrotational near field measure pressure induced by dynamics of the large-scale structures, but heavily weighted towards the largest scales (George, Beuther & Arndt 1984). Convection of these structures constitutes one leg of the feedback loop responsible for the screech. Azimuthal decomposition of the baseline pressure reveals that the two peaks at $St_D = 0.37$ and 0.47 are associated with $m = 1$ and 0 modes, respectively. The structures observed in the forced jet with St_{DF} of 0.13 in figure 7 are also suspected to be associated with the screech tone at St_D of 0.47. Note a down-shift in the broadband peak frequency at $x/D = 6$, corroborating the increased time scale (thus length scale) of the large-scale structures seen in figure 7(*a*).

The forcing tone appears in every excited jet spectrum, similarly to the far-field results, and is marked by a triangular symbol. At x/D of 3, all other peaks, except those marked by thin lines and the one at St_D of 0.88 in the spectrum with St_{DF} of 1.5, are harmonics of the forcing frequencies. The two main peaks in the baseline case are suppressed to various degrees by forcing up to St_{DF} of 0.68, but the one at $St_D \sim 0.47$ reappears when the jet is excited with St_{DF} of 0.95 and 1.5. In fact, the peak, which is also the subharmonic of the former, is significantly stronger than the one in the baseline. This peak also reappears at $x/D = 6$. Crow & Champagne (1971) observed a similar subharmonic growth when they forced a lower Re_D subsonic jet with turbulent initial shear layer at $St_{DF} = 0.6$. Zaman & Hussain (1980) in a subsonic jet with either laminar or tripped boundary layer observed vortex pairing when St_{DF} was 0.85. This vortex pairing occurred at $x/D \sim 2$. While we have not observed any vortex pairing in our flow visualizations due to difficulty in visualizing the jet near the nozzle exit, it appears from figure 8 that this is the same phenomenon. It seems that the extremely weak subharmonics in the current work are amplified when they coincide with the screech tone at $St_D \sim 0.47$. Unfortunately we do not have near-field pressure results for St_{DF} of 0.79, whose subharmonic of ~ 0.39 is close to the other screech tone. The peculiar behaviour both in the centreline TKE and the jet growth for St_{DF} of 0.79 shown in figure 6 could be related to this process of subharmonic formation. The results at x/D of 6 are similar, but with lower tonal amplitudes.

Figure 9 shows the changes due to forcing in the modal content of the irrotational near-field pressure fluctuations in comparison with the baseline case ($\Delta OASPL = OASPL_{excited} - OASPL_{baseline}$) where $OASPL$ is the overall sound pressure level. The Fourier azimuthal mode of the near-field pressure is denoted by m_p. Since the forcing is axisymmetric, the $OASPL$ of $m_p = 0$ was increased significantly for lower St_{DF} and peaked at St_{DF} of 0.41. Based on these results, the jet preferred mode Strouhal number seems to be around 0.41, not around 0.3 as was indicated by the far-field acoustic results or around 0.5 indicated by turbulence results (Kim & Samimy 2009). The results in the literature show significant variations in the jet preferred Strouhal number depending on what is measured and where it is measured (Crighton & Gaster 1976; Ho & Huerre 1984). The results at $x/D = 6$ show a similar trend.

3.3. *Excitation of $m = 3$ for noise mitigation*

In this section, we will present and discuss the results for $m = 3$ mode forcing. This is the highest simple azimuthal mode that can be forced with the eight actuators and provides the largest noise suppression. Detailed results for the excitation of $m = 1$ and

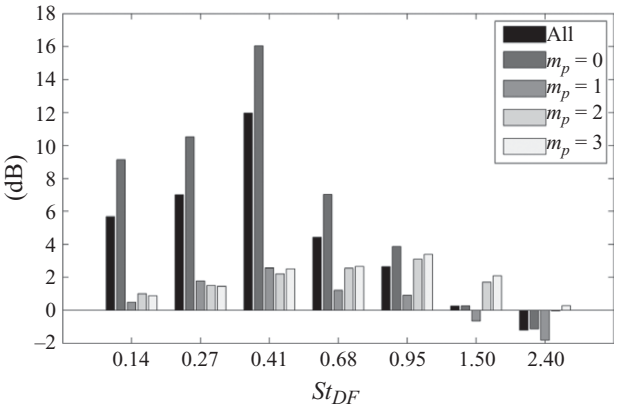

FIGURE 9. Changes relative to baseline flow in *OASPL* of the irrotational near-field pressure azimuthal modes (m_p) for the jet excited with $m = 0$ mode and several St_{DF} at $(x/D, r/D)$ of (3, 1.25).

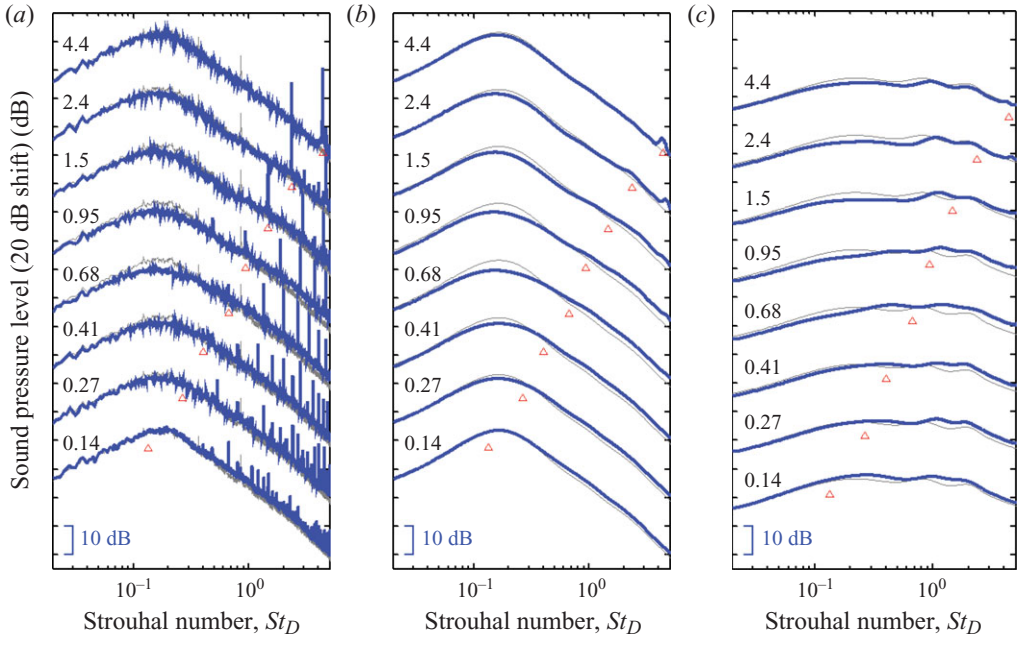

FIGURE 10. (Colour online) Far-field SPL at 30° (*a* and *b*) and 90° (*c*) for baseline jet (thin grey line) and $m = 3$ mode excitation over a large range of St_{DF}: (*a*) with excitation tones retained; (*b*, *c*) with excitation tones removed.

2 azimuthal modes will not be presented in the interest of brevity, but the overall sound pressure level results will be shown later in this section for all simple azimuthal modes.

3.3.1. *Far-field acoustic results*

Figures 10(*a*) and 10(*b*) show far-field acoustic spectra at 30° polar angle for $m = 3$ excitation over a large range of St_{DF}. The screech tones are suppressed, as they were in the $m = 0$ excitation case. Comparing the results with those of $m = 0$ mode

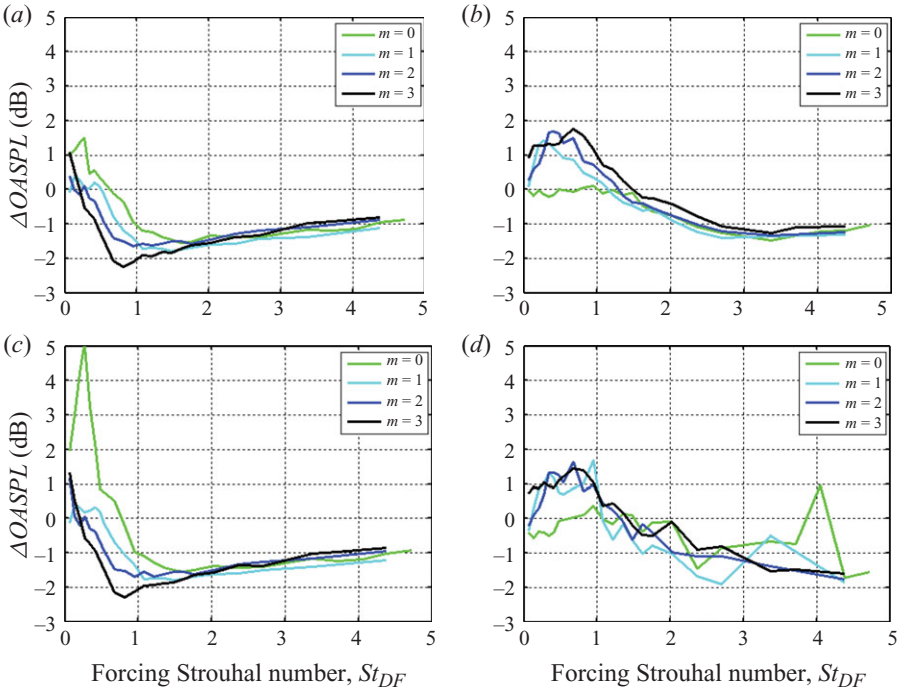

FIGURE 11. (Colour online) Far-field *OASPL* change at 30° (*a*, *c*) and 90° (*b*, *d*) for excitation of simple azimuthal modes without (*a*, *b*), and with (*c*, *d*) excitation tones.

excitation in figures 4 and 5, several differences are observed. First, the forcing tone does not appear at lower St_{DF}. Second, the broadband noise amplification at low St_{DF} is much lower in the $m = 3$ excitation case. Third, the noise suppression around the peak noise is significantly larger and starts at much lower St_{DF} in comparison with $m = 0$ excitation results. Maximum noise suppression is 4–5 dB at St_{DF} values 0.68–0.95. Finally, the St_{DF} for maximum noise mitigation is much lower for $m = 3$ mode excitation (0.95 versus ~ 2.0).

Figure 10(*c*) shows the far-field spectra at 90° polar angle. Both screech tones are suppressed (not shown), similar to the $m = 0$ excitation case and similar to the 30° polar angle results, the forcing tone does not appear at lower St_{DF}, but appears at higher St_{DF}. The broadband amplification level at lower St_{DF} and the broadband suppression level at higher St_{DF} are both higher than for the $m = 0$ case. It is speculated that the prolonged interaction and decay of weaker large-scale structures, in comparison with the $m = 0$ forcing case, generate more small-scale structures, dynamics of which radiate more noise to the sideline. Also, similar to the $m = 0$ case, the optimum St_{DF} for noise suppression is much higher than that at 30° polar angle (~ 1.5 versus ~ 0.95). Bechert & Pfizenmaier (1977) used four acoustic drivers to force $m = 1$ mode at St_{DF} of 0.3 in a Mach 0.6 jet. Their far-field results at 45° polar angle showed broadband amplification similar to that of $m = 0$ mode, but the forcing tone and its harmonics were weaker than those of $m = 0$ mode.

Figure 11 shows changes in the far-field overall sound pressure level ($\Delta OASPL = OASPL_{excited} - OASPL_{baseline}$) at 30° (figure 11*a* and figure 11*c*) and 90° (figure 11*b* and figure 11*d*) polar angles for excitation of $m = 0$–3 modes over a large range of St_{DF}. In calculating far-field *OASPL*, spectra are integrated over an

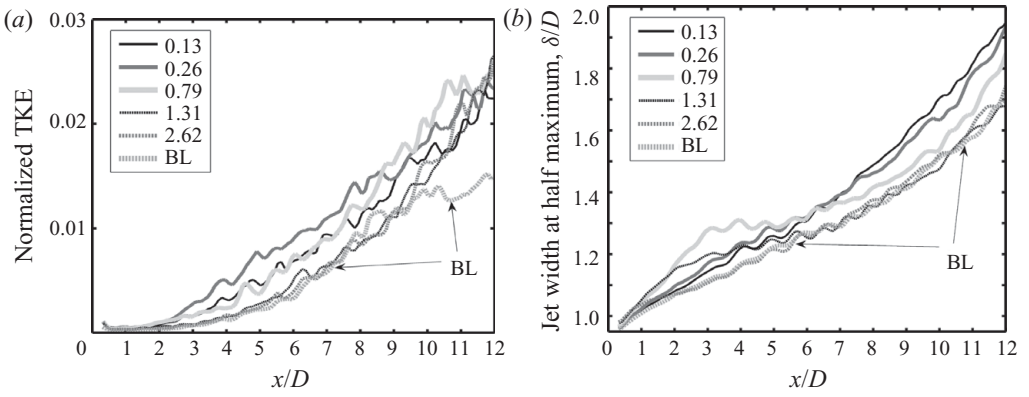

FIGURE 12. (*a*) Normalized centreline TKE, and (*b*) jet width, for baseline jet (BL) and excited jet with $m = 3$ for various St_{DF}.

St_D range of 0.01–4.0. The results are presented without (figure 11*a* and figure 11*b*) and with (figure 11*c* and figure 11*d*) the forcing tones. Retaining the forcing tone and its harmonics does not change the overall trend, but mainly increases $\Delta OASPL$ at 30° polar angle at low St_{DF}, especially in the $m = 0$ excitation case around the jet preferred St_D. Recall from figures 4 and 5 that there are many more tones at lower St_{DF}, especially in the $m = 0$ case, over the range of St_D used to calculate $\Delta OASPL$. Retaining the forcing tones also makes the graphs jagged at the 90° polar angle. There is a definite trend of larger noise suppression with higher azimuthal mode excitation at the 30° polar angle – noise suppression is the highest for $m = 3$ excitation, which is of course the highest simple forcing azimuthal mode obtainable with our eight actuators. The largest noise amplification is obtained with $m = 0$ excitation, which is almost exclusively used in the literature. The effects of different azimuthal modes become less distinguishable at higher St_{DF} and also at the 90° polar angle. Comparing these results with flow visualization results in figure 7, it appears that as long as the generated/manipulated large-scale structures are coherent (e.g. up to St_{DF} of 1.31), azimuthal modes play a role in noise amplification or suppression. These trends are similar to those observed in the excitation of a Mach 0.9 jet with Re_D of $\sim 630\,000$. However, the peak noise suppression was about 1 dB versus over 2 dB in the present case (Samimy *et al.* 2007*a*).

3.3.2. *Flow results*

Figure 12(*a*) shows jet normalized centreline TKE for the baseline jet and several forced jets with $m = 3$. Comparing these results with those presented in figure 6 for $m = 0$, the trends are quite similar. However, the centreline turbulence amplification is higher for St_{DF} of 0.13 than for 0.26. The jet centreline Mach number decay rate (not shown here) is also the highest with St_{DF} of 0.13. An analogous effect can be observed in the $\Delta OASPL$ results of figure 11(*a*), in which the maximum broadband amplification is shifted to a lower St_{DF}. Similar down-shift in the jet preferred mode St_D for higher azimuthal modes has also been observed in a Mach 0.9 jet (Kastner, Kim & Samimy 2009).

Figure 12(*b*) shows the jet width. Again, the trends are quite similar to those in figure 6 for $m = 0$ excitation, except for one significant difference: the roles of St_{DF} values of 0.79 and 1.31 are switched. The initial growth rate for the two lowest St_{DF}

is similar to the baseline case, but their further downstream growth rate is much higher. The initial growth rates for the other three cases are higher, but among them, the growth rates for St_{DF} of 0.79 and 1.31 are almost the same. However, the former has a longer and sustained initial growth. Recall from figures 10 and 11 that St_{DF} of around 0.79 is close to where the maximum noise suppression for $m = 3$ excitation takes place; for the $m = 0$ excitation, the corresponding Strouhal number is around 1.31. Note that we do not have an exact one-to-one correspondence between the flow and acoustic St_{DF}, so we are interpolating the results between the available data. Further downstream, the growth rate of the two highest St_{DF} cases is very similar to that of the baseline case. These results along with the results for $m = 0$ excitation seem to agree with the results in low Re_D jets (Zaman & Hussain 1981; Hussain & Hasan 1985) that the key for noise mitigation is to provide excitation that induces maximum initial jet growth rate. Apparently, this limits the downstream distance where the large-scale structures grow, saturate and start decaying and thus limits the extent of their dynamic interactions, which are believed to be a major jet noise source.

Phase-averaged qualitative flow images and conditionally averaged Galilean streamlines of the jet excited with $m = 3$ (not shown) confirmed the results shown in figure 12 that the jet responds better to St_{DF} of 0.13 than 0.26. However, the forcing wavelength and the wavelength of the structures do not match. The excitation of the axisymmetric mode of screech tone at $St_D \sim 0.47$ was offered as a possible source of the structures observed with $St_{DF} = 0.13$ in figure 7(*a*); the same phenomenon, but perhaps the excitation of $m = 1$ screech tone at $St_D \sim 0.37$, could be at work here as well. The results also showed that structures for St_{DF} of 0.79 and 1.31 are not as coherent as their counterparts in excitation of $m = 0$ mode (figure 7).

3.3.3. *Near-field pressure results*

Figure 13 shows pressure spectra for the baseline jet and excited jet with $m = 3$ mode for several St_{DF}. Again, the forcing tone, marked by a triangular symbol, appears in every excited jet spectrum, similar to the $m = 0$ excited results, but unlike the far-field results for $m = 3$ (figure 10), in which the forcing did not appear until St_{DF} of 0.68. However, the tonal amplitudes are much smaller in comparison with those in $m = 0$ mode excitation. The appearance of the excitation tones in the near-field but not in the far-field for $m = 3$ excitation mode is another sign of higher azimuthal modes being less efficient noise radiators, as has been remarked in the literature (Michalke & Fuchs 1975; Hall *et al.* 2006). Similar to the $m = 0$ excitation case, the tones associated with the screech modes are suppressed. Note also the existence of the subharmonic of the forcing tone at St_{DF} of 0.95 (as was observed in figure 8 for $m = 0$ excitation) and at St_{DF} of 1.5.

4. Concluding remarks

The effects of forcing over a wide range of St_{DF} and azimuthal modes on the far-field acoustic, flow velocity and irrotational near-field pressure of an axisymmetric perfectly expanded Mach 1.3 jet with Re_D of 1.1×10^6 and a turbulent boundary layer at the nozzle exit were explored. The objectives were three-fold: (i) to investigate the broadband far-field noise amplification reported in the literature using excitation of $m = 0$ at St_{DF} straddling the jet column mode; (ii) to explore broadband far-field noise suppression using excitation of higher values of m and St_{DF}; and (iii) to shed some light on the connection between the flow field and the far-field noise.

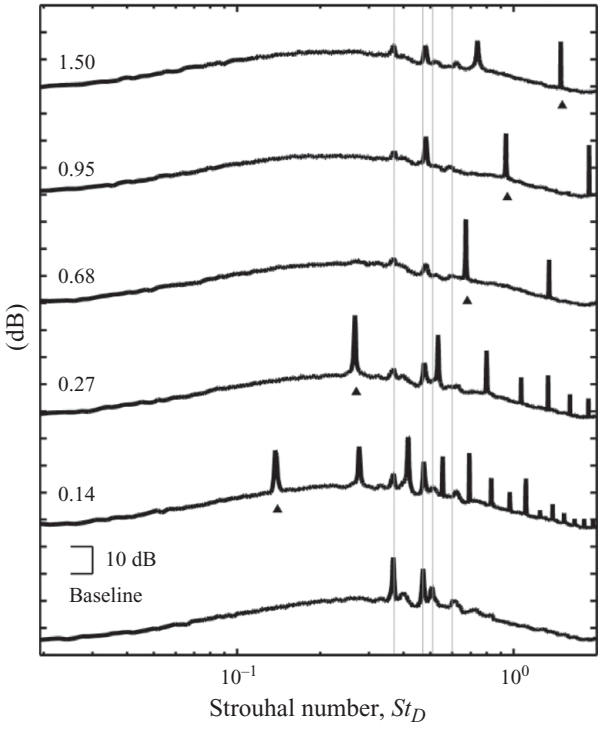

FIGURE 13. Near-field pressure spectra for the baseline jet and excited jet with $m = 3$ mode for several St_{DF} at $(x/D, r/D)$ of (3, 1.25).

The results show significant similarities with those in relatively low-speed and low Re_D jets. For $m = 0$ excitation, amplifications of far-field noise, irrotational near-field pressure and broadband turbulence were observed at low St_{DF}. The broadband far-field noise amplification due to forcing near the jet preferred mode of ~ 0.3 was not as extensive in amplitude or frequency as in the low-speed and low Re_D jet, but still large enough to be perhaps a concern in practical applications. When the jet was forced with an St_D whose harmonic was within the jet column St_D, a sign of vortex pairing was evident in the near-field pressure. Coherent structures were observed in the forced jet over a wide range of St_{DF} (up to ~ 1.31) with the largest and most organized structures around the jet preferred mode St_D. Significant variations in the jet preferred mode St_D was observed depending upon what was used to determine it.

Significant broadband noise suppression was achieved with excitation of $m = 3$ over a large range of St_{DF} with peak suppression of 4–5 dB at the 30° polar angle peak frequency resulting in approximately 2 dB suppression in the overall sound pressure level at $St_{DF} \sim 0.9$. The excitation tone and its harmonics were observed for both $m = 0$ and $m = 3$ excitation in the irrotational near-field pressure spectra. They also appeared in the far-field acoustic spectra at almost all St_{DF} in $m = 0$, but only at higher St_{DF} in $m = 3$. These results confirm that, even in this very high Re_D supersonic jet, $m = 0$ is an efficient far-field radiator while $m = 3$ is not as efficient. When noise suppression was achieved using higher St_{DF} and azimuthal modes, the nature of the jet growth was similar to that of a low Re_D and low-speed jet forced with the maximum jet growth rate $St_{\theta F}$.

Of the structure-based noise sources discussed earlier, the only one that can be easily ruled out is the pairing, as either it does not exist in such a high-speed and high Re_D jet, or even when it exists it occurs very close to the nozzle exit while the main noise sources are further downstream. Of the growing, saturation and decaying phases of coherent wave packets, instability waves or structures, it is difficult to assess which phase is more important. Kastner *et al.* (2009) reported that in a Mach 0.9 jet, the noise source distribution is almost Gaussian, with a peak between 6 and 9 jet diameters, and the peak is shifted only by a couple of jet diameters using various forcing. Based on the results reported here, one can speculate that three important factors in reducing noise are (i) controlling the size of the structures; (ii) limiting the spatial extent of their growth; and (iii) reducing interaction between the structures.

The support of this research by NASA Glenn Research Center with James Bridges and Cliff Brown is greatly appreciated. The help and support of Igor Adamovich and Munetake Nishihara have been instrumental. We have had fruitful discussions with James Bridges, Dan Bodony, Jon Freund, Fazle Hussain, Jeff Kastner and Khairul Zaman.

REFERENCES

Ahuja, K. K. 1985 Some unique experiments on receptivity. *AIAA Paper 85-0533.*

Ahuja, K. K. & Blakney, D. F. 1985 Tone excited jets. Part IV. Acoustic measurements. *J. Sound Vib.* **102** (1), 93–117.

Alkislar, M. B. 2009 Flow characteristics of a jet controlled with Chevron–Microjet combination for noise reduction. In *Forty-seventh AIAA Aerospace Sciences Meeting. AIAA Paper 2009-851.*

Arakeri, V. H., Krothapalli, A., Siddavaram, V., Alkislar, M. B. & Lourenco, L. M. 2003 On the use of microjets to suppress turbulence in a Mach 0.9 axisymmetric jet. *J. Fluid Mech.* **490**, 75–98.

Barone, M. F. & Lele, S. K. 2005 Receptivity of the compressible mixing layer. *J. Fluid Mech.* **540**, 301–335.

Bechert, D. W. 1988 Excitation of instability waves in free shear layers. Part 1. Theory. *J. Fluid Mech.* **188**, 47–62.

Bechert, D. W. & Pfizenmaier, E. 1975 On the amplification of broadband jet noise by a pure tone excitation. *J. Sound Vib.* **43** (3), 581–587.

Bechert, D. W. & Pfizenmaier, E. 1977 Amplification of jet noise by a higher-mode acoustical excitation. *AIAA J.* **15** (9), 1268–1271.

Bechert, D. W. & Stahl, B. 1988 Excitation of instability waves in free shear layers. Part 2. Experiments. *J. Fluid Mech.* **188**, 63–84.

Bridges, J. E. & Hussain, A. K. M. F. 1987 Roles of initial condition and vortex pairing in jet noise. *J. Sound Vib.* **117** (2), 289–311.

Bridges, J. E. & Hussain, A. K. M. F. 1992 Direct evaluation of aeroacoustic theory in a jet. *J. Fluid Mech.* **240**, 469–501.

Brown, G. L. & Roshko, A. 1974 On density effects and large structure in turbulent mixing layers. *J. Fluid Mech* **64** (4), 715–816.

Castelain, T., Sunyach, M., Juve, D. & Bera, J.-C. 2007 Jet noise reduction by impinging microjets: an aerodynamic investigation testing microjet parameters. In *Thirteenth AIAA/CEAS Aeroacoustics Conference. AIAA Paper 2007-3419.*

Cohen, J. & Wygnanski, I. 1987 The evolution of instabilities in the axisymmetric jet. Part 1. The linear growth of disturbances near the nozzle. *J. Fluid Mech.* **176**, 191–219.

Corke, T. C., Shakib, F. & Nagib, H. M. 1991 Mode selection and resonant phase locking in unstable axisymmetric jets. *J. Fluid Mech.* **223**, 253–311.

Crighton, D. G. 1981 Jet noise and the effects of jet forcing. In *The Role of Coherent Structures in Modeling Turbulence and Mixing* (ed. J. Jimenez). Lecture Notes in Physics, vol. 136, pp. 340–362. Springer.

Crighton, D. G. 1985 The Kutta condition in unsteady flow. *Annu. Rev. Fluid Mech.* **17**, 411–445.

Crighton, D. G. & Gaster, M. 1976 Stability of slowly diverging jet flow. *J. Fluid Mech.* **77** (2), 387–413.

Crow, S. & Champagne, F. 1971 Orderly structure in jet turbulence. *J. Fluid Mech.* **48** (3), 547–591.

Deneuville, P. & Jacques, J. 1977 Jet noise amplification: a practically important problem. *AIAA Paper 77-1362.*

Ffowcs-Williams, J. E. & Kempton, A. J. 1978 The noise from the large-scale structure of a jet. *J. Fluid Mech.* **84** (4), 673–694.

George, W. K., Beuther, P. D. & Arndt, R. E. A. 1984 Pressure spectra in turbulent free shear flows. *J. Fluid Mech.* **148**, 155–191.

Gudmundsson, K. & Colonius, T. 2009 Parabolized stability equation models for turbulent jets and their radiated sound. In *Fifteenth AIAA/CEAS Aeroacoustics Conference. AIAA Paper 2009-3380.*

Hall, J., Pinier, J., Hall, A. M. & Glauser, M. N. 2006 Two-point correlations of the near-field and far-field pressure in a transonic jet. In *Proceedings of the Fluids Engineering Summer Meeting (FEDSM2006-98458)*, Miami, Fl. ASME.

Hileman, J., Thurow, B. S., Caraballo, E. J. & Samimy, M. 2005 Large-scale structure evolution and sound emission in high-speed jets: real-time visualization with simultaneous acoustic measurements. *J. Fluid Mech.* **544**, 277–307.

Ho, C.-M. & Huerre, P. 1984 Perturbed free shear layers. *Annu. Rev. Fluid Mech.* **16**, 365–424.

Hussain, A. K. M. F. 1983 Coherent structures – reality and myth. *Phys. Fluids* **26** (10), 2816–2850.

Hussain, A. K. M. F. 1986 Coherent structures and turbulence. *J. Fluid Mech.* 173, 303–356.

Hussain, A. K. M. F. & Hasan, M. A. Z. 1985 Turbulence suppression in free turbulent shear flows under controlled excitation. Part 2. Jet-noise reduction. *J. Fluid Mech.* **150**, 159–168.

Jordan, P. & Gervais, Y. 2008 Subsonic jet aeroacoustics: associating experiment, modelling and simulation. *Exp. Fluids* **44**, 1–21.

Jubelin, B. 1980 New experimental studies on jet noise amplification. *AIAA Paper 1980-0961.*

Kastner, J., Kim, J.-H. & Samimy, M. 2009 A study of the correlation of large-scale structure dynamics and far-field radiated noise in an excited Mach 0.9 jet. *Intl J. Aeroacoust.* **8** (3), 231–159.

Kearney-Fischer, M., Kim, J.-H. & Samimy, M. 2009*a* Noise control of a high Reynolds number Mach 0.9 heated jet using plasma actuators. *AIAA Paper 2009-3188.*

Kearney-Fischer, M., Kim, J.-H. & Samimy, M. 2009*b* Control of a high Reynolds number Mach 0.9 heated jet using plasma actuators. *Phys. Fluids* **21**, 095101.

Kibens, V. 1980 Discrete noise spectrum generated by an acoustically excited jet. *AIAA J.* **18** (4), 434–451.

Kim, J.-H., Kastner, J. & Samimy, M. 2009*a* Active control of a high Reynolds number Mach 0.9. *AIAA J.* **47** (1), 116–128.

Kim, J.-H., Nishihara, M., Keshav, S., Adamovich, I., Samimy, M., Gorbatov, S. V. & Pliavaka, F. V. 2009*b* On the development of localized arc filament plasma actuators for high-speed flow control. *AIAA Paper 2009-4071.*

Kim, J.-H. & Samimy, M. 2009 Effects of active control on the flow structure in a high Reynolds number supersonic jet. *Intl J. Flow Control* **1** (2), 99–117.

Lighthill, M. J. 1952 On sound generated aerodynamically. Part I. General theory. *Proc. R. Soc. Lond.* A **211** (1107), 564–587.

Lu, H. Y. 1983 Effects of excitation on coaxial jet noise. *AIAA J.* **21** (2), 214–220.

Michalke, A. 1965 On spatially growing disturbances in an inviscid shear layer. *J. Fluid Mech.* **23** (3), 521–544.

Michalke, A. & Fuchs, H. V. 1975 On turbulence and noise of an axisymmetric shear flow. *J. Fluid Mech.* **70** (1), 179–205.

Moore, C. J. 1977*a* The role of shear-layer instability waves in jet exhaust noise. *J. Fluid Mech.* **80** (2), 321–367.

Moore, C. J. 1977*b* The effect of shear layer instability on jet exhaust noise. In *Structure and Mechanisms of Turbulence* (ed. H. Fiedler). Lecture Notes in Physics, Springer.

Morrison, G. & McLaughlin, D. 1979 Noise generation by instabilities in low Reynolds number supersonic jets. *J. Sound Vib.* **65** (2), 177–191.

Norum, T. D. 1983 Screech suppression in supersonic jets. *AIAA J.* **21** (2), 235–240.

Raman, G. 1999 Supersonic jet screech: half-century from Powell to the present. *J. Sound Vib.* **225** (3), 543–571.

Reba, R., Narayanan, S., Colonius, T. & Suzuki, T. 2005 Modeling jet noise from organized structures using near-field hydrodynamic pressure. In *Eleventh AIAA/CEAS Aeroacoustics Conference. AIAA Paper* 2005-3093.

Samimy, M., Adamovich, I., Webb, B., Kastner, J., Hileman, J., Keshav, S. & Palm, P. 2004 Development and characterization of plasma actuators for high speed jet control. *Exp. Fluids* **37** (4), 577–588.

Samimy, M., J., Kim, Kastner, J.-H., Adamovich, I. & Utkin, Y. 2007*a* Active control of a Mach 0.9 jet for noise mitigation using plasma actuators. *AIAA J.* **45** (4), 890–901.

Samimy, M., Kim, J.-H., Kastner, J., Adamovich, I. & Utkin, Y. 2007*b* Active control of high speed and high Reynolds number jets using plasma actuators. *J. Fluid Mech.* **578**, 305–330.

Suzuki, T. & Colonius, T. 2006 Instability waves in a subsonic round jet detected using a near-field phased microphone array. *J. Fluid Mech.* **565**, 197–226.

Tam, C. K. W. 1978 Excitation of instability waves in a two-dimensional shear layer by sound. *J. Fluid Mech.* **89** (2), 357–371.

Tam, C. K. W. 1998 Jet noise: since 1952. *Theor. Comput. Fluid Dyn.* **10**, 393–405.

Tanna, H. K. & Ahuja, K. K. 1985 Tone excited jets. Part I. Introduction. *J. Sound Vib.* **102** (1), 57–61.

Tinney, C. E. & Jordan, P. 2008 The near pressure field of co-axial subsonic jets. *J. Fluid Mech.* **611**, 175–204.

Utkin, Y. G., Keshav, S., Kim, J.-H., Kastner, J., Adamovich, I. V. & Samimy, M. 2007 Development and use of localized arc filament plasma actuators for high-speed flow control. *J. Phys.* D*: Appl. Phys.* **40**, 685–694.

Zaman, K. B. M. Q. & Hussain, A. K. M. F. 1980 Vortex pairing in a circular jet under controlled excitation. Part 1. General jet response. *J. Fluid Mech.* **101** (3), 449–491.

Zaman, K. B. M. Q. & Hussain, A. K. M. F. 1981 Turbulence suppression in free shear flows by controlled excitation. *J. Fluid Mech.* **103**, 133–159.